International Journal of Energy and Environmental Science
2026, Vol. 11, No. 6, pp. 152–159
https://doi.org/10.11648/j.ijees.20261106.12

SciencePG
Science Publishing Group

Research Article

Effects of Oil-Soluble Molybdenum Catalysts on the Molecular Composition and Lightening Performance of Residue Slurry-Phase Hydrocracking Products

Yidi Wang, Bin Liu, Yongming Chai*

College of Chemistry and Chemical Engineering, China University of Petroleum (East China), Qingdao, China

Abstract

Using A1VR, 941VR, M16VR, and HybridVR residues as feedstocks, the slurry-phase hydrocracking performance of two oil-soluble molybdenum catalysts, OMO and OMS, was systematically investigated. The effects of catalyst type on product composition and boiling-range distribution were evaluated by gas chromatography-mass spectrometry (GC-MS) and simulated distillation. The results showed that the saturated and aromatic hydrocarbon fractions of all four feedstocks exhibited pronounced unresolved complex mixture (UCM) backgrounds, reflecting the complex molecular composition of heavy petroleum fractions. Following slurry-phase hydrocracking, the chromatograms showed enhanced discrete peaks in the low-retention-time region and a substantial attenuation of the broad UCM backgrounds in the high-retention-time region. These changes indicated the conversion of heavy molecular components into lighter hydrocarbons through chain scission, depolymerization, and hydrogenation stabilization. In particular, the transformations of resins, asphaltenes, and condensed-ring aromatic compounds contributed to the reduction of heavy components and the formation of lower-carbon-number products. Compared with OMO, OMS exhibited a more pronounced upgrading effect, as evidenced by stronger light-hydrocarbon peak groups and greater attenuation of the high-retention-time UCM backgrounds. Notably, the broad chromatographic background of 941VR was almost completely eliminated after treatment with OMS, suggesting a substantial conversion of its heavy molecular components. Simulated distillation results further confirmed the superior upgrading performance of OMS, which produced higher gasoline and diesel yields while reducing the proportions of wax oil and residue. For HybridVR, the total light fraction yield increased from 38.80 wt% to 54.59 wt% after hydrocracking with OMS, demonstrating its effectiveness in promoting residue conversion and liquid product recovery. The enhanced catalytic performance of OMS is attributed to its ability to rapidly generate highly dispersed MoS_2 active phases with abundant exposed edge sites. These active sites facilitate hydrogen activation and the stabilization of free radicals generated during thermal cracking, thereby suppressing radical recombination and condensation reactions while promoting the conversion of heavy molecular structures. Overall, OMS demonstrates considerable potential for improving the slurry-phase hydrocracking performance of different vacuum residues, particularly in terms of heavy-component conversion, residue lightening, and the enhancement of valuable light fractions.

Keywords

Oil-soluble Mo Catalysts, GC-MS, Slurry Phase, Residue

*Correspondence: Yongming Chai (ymchai@upc.edu.cn)

Received: 21 October 2026; **Accepted:** 3 November 2026; **Published:** 25 November 2026

Copyright: © The Author(s), 2026. Published by Science Publishing Group. This is an **Open Access** article, distributed under the terms of the Creative Commons Attribution 4.0 License (http://creativecommons.org/licenses/by/4.0/), which permits unrestricted use, distribution and reproduction in any medium, provided the original work is properly cited.

1. Introduction

With the increasing trend of heavy and inferior crude oils, the efficient lightening of residue has become an important challenge facing the refining industry [1-4]. Residue is enriched with large amounts of resins, asphaltenes, and highly condensed polycyclic aromatic hydrocarbons. These components have high molecular weights and complex structures and form three-dimensional associated structures through alkyl bridges, methylene bridges, and heteroatom bridges, which are the main factors causing the refractory nature of residue and the relatively low yield of light oils. Slurry-phase hydrocracking has the characteristics of strong feedstock adaptability, high conversion depth, and good coke suppression ability, and is an important technological pathway for the deep conversion of heavy oils. In this process, heavy macromolecules first undergo thermal cracking to generate radical intermediates, which are then stabilized by active hydrogen provided at catalyst active sites, followed by reactions such as chain scission, dealkylation, and hydrogenation saturation, thereby achieving targeted conversion toward light fractions [2-5]. Therefore, the active-phase formation rate, dispersibility, and hydrogen-donating ability of the catalyst directly affect the conversion depth of heavy components and the product distribution.

Oil-soluble molybdenum catalysts have attracted widespread attention because of their good dispersibility in residue and high hydrogenation activity. Among them, the oil-soluble molybdenum carboxylate precursor (OMO) requires ligand thermal decomposition, sulfidation, and active-phase reconstruction before MoS2 active structures can be formed, and thus has a certain activation induction period; in contrast, the oil-soluble self-sulfiding molybdenum disulfide precursor (OMS) can rapidly form a highly dispersed MoS2 active phase under reaction conditions and theoretically possesses stronger hydrogen activation and radical stabilization abilities [6]. However, systematic comparative studies on the differences between these two types of catalysts in the evolution of saturated and aromatic hydrocarbon molecular compositions and in the fraction distribution during slurry-phase hydrocracking of various typical residues are still lacking [7-11].

On this basis, four typical residues, A1VR, 941VR, M16VR, and HybridVR, were used as feedstocks in this study to compare the slurry-phase hydrocracking products catalyzed by OMO and OMS. By combining GC-MS semi-quantitative analysis, total ion chromatograms of saturated and aromatic hydrocarbons, and high-temperature simulated distillation, the variation patterns of hydrocarbon composition, heavy-component conversion, and fraction distribution before and after hydrogenation were investigated, and the differences in the effects of the two oil-soluble molybdenum catalysts on the migration of the residue molecular weight distribution toward the lower-carbon-number region were revealed, providing a basis for the design of high-performance catalysts for slurry-phase residue hydrocracking and for the efficient lightening of heavy oils [12-15].

2. Materials and Methods

Two types of catalysts were employed in this work, namely an oxidized oil-soluble molybdenum isooctanoate catalyst (OMO) and a presulfided oil-soluble MoS_2 catalyst (OMS). The four typical residues are A1VR, 941VR, M16VR, and HybridVR. A Thermo Scientific Trace 1310 GC coupled with a Thermo Scientific TSQ 8000Evo MS was used for the analysis of aromatic fractions. The GC was equipped with a HP-5MS (60 m × 0.25 mm × 0.25 μm) fused silica capillary column. Oven temperature was programed from 50 to 120℃ at 15 ℃/min and 120 to 300 ℃ at 3 °C/min with an initial hold time of 1 min and a final hold time of 35 min [16]. The energy of electron ionization (EI) source was 70 eV and it was operated at 230 ℃. The mass range of aromatic fraction analysis was from m/z 35 to m/z 420 with 0.92 s [5-9]. A LECO Pegasus 4D GC×GC-TOF MS system (LECO Corporation, USA) was used for the analysis, and data processing was performed with Chroma TOF software (LECO Corporation) The first-dimension column was a DB-5Q (30 m × 0.2 mm × 0.25 μm). The primary oven temperature was programmed as follows: held at 50 ℃ for 1 min, then ramped to 240 ℃ at 2 ℃/min. The second-dimension column was a DB-17HT (1.2 m ×0.18 mm × 0.18 μm), with a secondary oven temperature offset of +10 ℃. The modulation period was 6 s. Helium (purity 99.995%) was used as the carrier gas in constant-flow mode at a flow rate of 1.0 mL/min. The injector temperature was 280°C, and 0.2 μL of sample was injected with a split ratio of 100:1. The mass spectrometer was equipped with an electron ionization (EI) source operated at 70 eV. The transfer line temperature was 280 ℃ and the ion source temperature was 250 ℃. Mass spectra were acquired in full-scan mode over the m/z range of 33–500 at an acquisition rate of 100 spectra per second [11-15].

3. Results and Discussion

Based on the GC-MS semi-quantitative analysis results, the saturated hydrocarbon compositions of different residue feedstocks and their hydrocracking products showed significant differences. Figures 1 and 2 show the GC-MS total ion chromatograms of saturated hydrocarbons in A1VR, 941VR, M16VR, and HybridVR feedstocks and in their hydrogenation products obtained with different catalysts. All chromatograms exhibit the coexistence of broad diffuse peaks and a small number of discrete peaks. The four feedstocks show a relatively obvious unresolved complex mixture (UCM) background after a retention time of 20 min, indicating that the feedstocks contain large amounts of high-carbon-number alkanes, cycloalkanes, and structurally complex heavy saturated components. In contrast, after hydrocracking, the product chromatograms of both the OMO and OMS catalytic systems show markedly enhanced discrete-peak features, especially numerous regularly distributed chromatographic peaks in the 5–35 min range, indicating that high-molecular-weight

saturated hydrocarbons underwent chain scission and cracking to varying degrees, producing more medium- and low-carbon-number n-alkane products. At the same time, the UCM background widely present in the feedstocks is significantly weakened, indicating that heavy components were effectively converted.

Further comparison of the variation patterns among different feedstocks shows that the A1VR feedstock originally had relatively few detectable light saturated hydrocarbon peaks, whereas after slurry-phase hydrocracking it formed a continuous and regular n-alkane peak series, indicating that its heavy components underwent relatively sufficient cracking. The change in the 941VR feedstock was the most significant: its feedstock chromatogram had the strongest diffuse background in the 20–50 min region, indicating a relatively high content of high-molecular-weight and compositionally complex matrix, whereas after hydrocracking this broad-peak background was greatly attenuated and numerous discrete peaks were released, indicating that high-molecular-weight components were deeply converted into separable low-molecular hydrocarbons. The M16VR feedstock itself had a relatively abundant medium-carbon-number alkane distribution; after hydrocracking, the peak shapes became sharper and the peak intensities increased significantly, reflecting further cracking of heavy components and migration toward a lower carbon-number range. The mixed VR feedstock combined the characteristics of the above feedstocks, and its hydrocracking products likewise showed the pattern of enhanced peak groups in the low-retention-time region and weakened background in the high-retention-time region. From the perspective of molecular composition evolution, this change reflects the trend in residue slurry-phase hydrocracking that large-molecular heavy components are dismantled and continuously migrate toward lower-carbon-number species. Under high-temperature and high-pressure hydrogen conditions, macromolecular associates such as resins and asphaltenes in heavy oil first undergo thermal cracking to generate radical intermediates, which are then rapidly stabilized by active hydrogen at catalyst active sites to form a series of lower-carbon-number n-alkanes and isoalkanes. Therefore, the large increase in regular peak groups in the product chromatograms actually represents the synergistic enhancement of thermal cracking and hydrogenation activity. Meanwhile, the complex heavy background in the feedstocks is significantly weakened, indicating that the catalytic system effectively suppresses radical condensation and secondary polymerization reactions and reduces the residual heavy components. Overall, the saturated hydrocarbon GC-MS results indicate that both oil-soluble molybdenum catalysts can promote the conversion of heavy components into light saturated hydrocarbons and achieve a shift of the residue molecular weight distribution toward the lower-carbon-number region, and this phenomenon is also an important manifestation of heavy-oil lightening by slurry-phase hydrocracking.

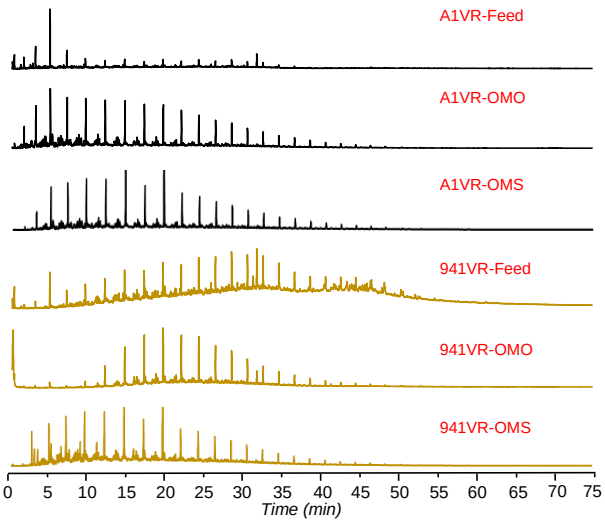

Figure 1. *GC-MS chromatograms of saturated hydrocarbons in A1VR and 941VR and the related hydrogenation products.*

Although both the OMO and OMS catalytic systems can promote the cracking conversion of heavy components in residue, judging from the magnitude of the GC-MS chromatographic changes, the OMS system exhibits stronger hydrocracking ability and a higher conversion depth of heavy components. Among the four feedstocks A1VR, 941VR, M16VR, and HybridVR, the OMS products all show more obvious enhancement of low-retention-time peak groups, while the attenuation of the diffuse background in the high-retention-time region is also significantly greater than that of the OMO system. Especially in the 941VR system, OMS almost completely eliminated the large-area broad-peak background in the 20–50 min region of the feedstock, whereas the OMO system still retained a certain degree of heavy-signal residue, indicating that OMS has stronger cracking conversion ability for high-molecular-weight saturated hydrocarbons and complex cyclic structures. In addition, the peak heights and peak areas of the continuous n-alkane peaks in the OMS products are generally higher than those in the OMO system, indicating that it can generate more light and middle-distillate hydrocarbons, which indirectly reflects a higher cracking depth and stronger hydrogenation stabilization ability. This difference is closely related to the formation mode of the active phases of the two catalysts. OMO is essentially an oil-soluble molybdenum carboxylate precursor, which must undergo steps such as ligand thermal decomposition, sulfidation, and active-phase reconstruction during the reaction before catalytically active MoS_2 nanostructures can be formed. Therefore, there is a certain activation induction period in the early stage of the reaction, and some molybdenum species may reduce the number of effective active sites due to incomplete sulfidation or local aggregation. In contrast, OMS is an oil-soluble self-sulfiding molybdenum disulfide precursor, which can more rapidly form a highly dispersed MoS_2 active phase under reaction

conditions, reducing structural loss and agglomeration during activation. The edge sites of highly dispersed MoS_2 nanosheets are key sites for hydrogen dissociation and active hydrogen generation in hydrocracking reactions; therefore, OMS more readily forms edge-rich active structures, thereby improving hydrogen activation ability.

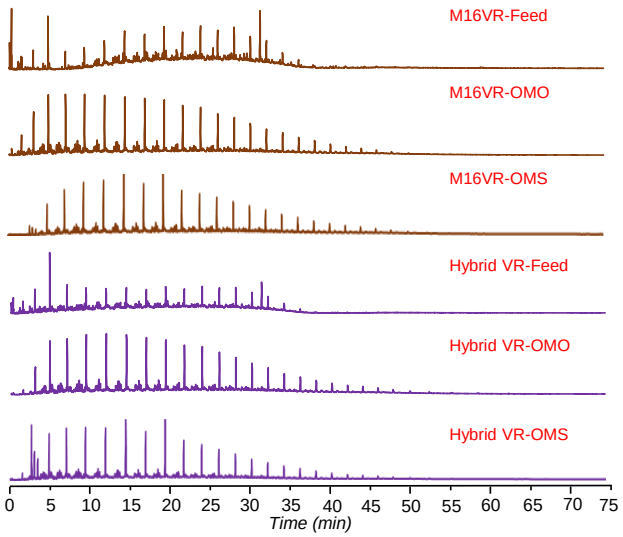

Figure 2. *GC-MS total ion chromatograms of saturated hydrocarbons in M16VR and HybridVR and the related hydrogenation products.*

In residue slurry-phase hydrocracking, a large number of radical intermediates are first generated in the reaction system under the action of thermal cracking, and these radicals have two competing reaction pathways: one is rapid quenching and stabilization by active hydrogen to form small-molecule hydrocarbons; the other is condensation, aromatization, and polymerization to form heavier condensed structures or even coke precursors. Because the OMS system can continuously provide a higher concentration of active hydrogen, radicals are more easily terminated by rapid hydrogenation, thereby promoting the stable existence of cracked products and allowing subsequent hydrocracking reactions to continue. At the same time, an adequate supply of active hydrogen can also inhibit condensation reactions between radicals and reduce the probability of condensation of heavy components. Therefore, in the saturated hydrocarbon GC-MS spectra, low-carbon-number alkane peaks increase significantly, while the heavy background in the high-retention-time region decreases markedly. By comparison, although the OMO system also has a certain hydrocracking ability, its active-phase formation rate and hydrogen activation ability are relatively weaker, and some cracked intermediates are difficult to stabilize in time, resulting in more residual heavy components. Overall, through more efficient MoS_2 active-phase formation, stronger hydrogen activation ability, and better radical stabilization, OMS achieves deeper hydrocracking and more thorough heavy-oil lightening than OMO.

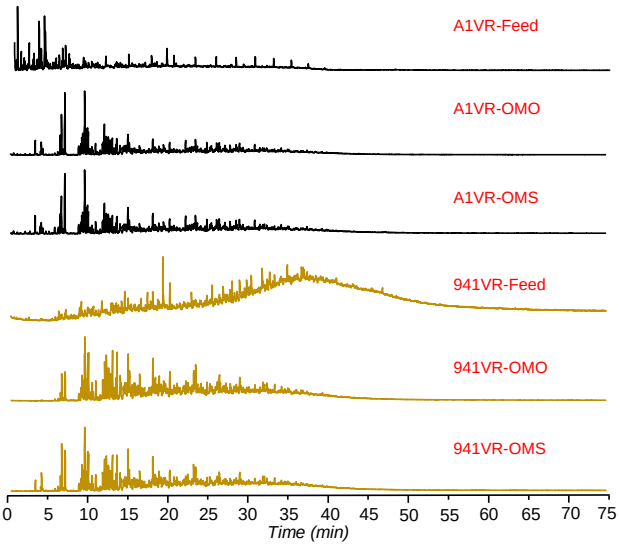

Figure 3. *GC-MS chromatograms of aromatic hydrocarbons in A1VR and 941VR and the related hydrogenation products.*

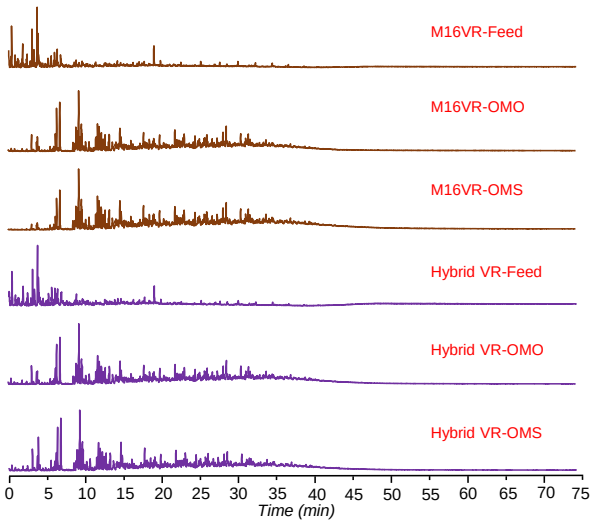

Figure 4. *GC-MS chromatograms of aromatic hydrocarbons in M16VR and HybridVR and the related hydrogenation products.*

Figures 3 and 4 show the GC-MS total ion chromatograms of aromatic hydrocarbons in A1VR, 941VR, M16VR, and HybridVR feedstocks and in their hydrogenation products obtained with different catalysts. The semi-quantitative analysis results indicate that the aromatic compound compositions and distribution characteristics of the different residue feedstocks and their hydrocracking products all changed significantly. As can be seen from the feedstock spectra, the four typical residue feedstocks all exhibited relatively broad chromatographic dis-

tribution ranges. Among them, the 941VR feedstock was particularly prominent, with obvious broad peaks and continuous background signals in the retention time region of 20–50 min, indicating that the system was enriched with large amounts of high-molecular-weight aromatic compounds and condensed aromatic structures derived from heavy components such as resins and asphaltenes. These components are usually composed of polycyclic aromatic hydrocarbons (PAHs), alkyl-substituted condensed-ring aromatic hydrocarbons, and some aromatic resin and asphaltene fragments; they have relatively high molecular weights and aromatic condensation degrees and are one of the main sources of the refractory nature of residue. In contrast, although the A1VR and M16VR feedstocks also showed obvious characteristic aromatic peaks, their diffuse background in the high-retention-time region was relatively weak, indicating that their heavy aromatic component contents were slightly lower than that of 941VR.

After slurry-phase hydrocracking, all samples showed a trend of aromatic composition migrating toward the low-retention-time region. The large-molecular aromatic components in the high-retention-time region of the feedstocks decreased markedly, while the number and intensity of discrete peaks in the retention time range of 5–20 min increased significantly. This indicates that resins, asphaltenes, and highly condensed aromatic structures underwent effective cracking during hydrocracking, generating more low-molecular-weight monocyclic, bicyclic, and some tricyclic aromatic hydrocarbons. Especially in the 941VR system, the large-area broad peaks in the 30–50 min region of the feedstock spectrum were significantly attenuated after the reaction, while numerous discrete peaks appeared in the low-retention-time region, indicating that the condensed-ring aromatic structures originally derived from resins and asphaltenes underwent deep conversion. The mixed VR feedstock also showed similar changes: the relatively flat background signal in its feedstock was transformed into numerous regular peak groups after hydrocracking, indicating that complex aromatic structures were continuously depolymerized and lightened. From a molecular perspective, resins and asphaltenes in residue are usually composed of aromatic cores linked by alkyl bridges, methylene bridges, and heteroatom bridges such as sulfur, nitrogen, and oxygen to form three-dimensional aggregate structures. During hydrocracking, these lower-bond-energy linking bonds first break, releasing smaller-molecular-weight aromatic structural units; subsequently, under the action of active hydrogen, dealkylation, partial hydrogenation saturation, and further cracking reactions occur, gradually converting highly condensed aromatic structures into lower-condensation-degree aromatic hydrocarbons. Therefore, the weakening of the broad-peak background in the high-retention-time region of the chromatograms actually reflects the continuous conversion of heavy components such as resins and asphaltenes into volatile and detectable small-molecule aromatic hydrocarbons. At the same time, some condensed-ring aromatic hydrocarbons may also undergo aromatic-ring hydrogenation to form hydroaromatic and naphthenoaromatic hydrocarbons, thereby further promoting the migration of heavy components toward light fractions. Overall, the GC-MS results fully demonstrate that both oil-soluble molybdenum catalysts can promote the depolymerization and conversion of aromatic resin and asphaltene structures in residue and achieve the targeted dismantling of aromatic heavy components into low-molecular-weight aromatic hydrocarbons.

Further comparison of the OMO and OMS catalytic systems shows that although both catalysts can effectively promote the conversion of aromatic heavy components, the OMS system exhibits a more significant hydrocracking effect. For the four feedstocks A1VR, 941VR, M16VR, and HybridVR, the OMS products all showed stronger low-retention-time aromatic peaks and lower high-retention-time background signals. Especially in the 941VR system, the large-area broad peaks of the feedstock almost completely disappeared under OMS catalysis, whereas a certain degree of heavy aromatic background was still retained in the OMO product. This indicates that OMS can more effectively crack the large-molecular aromatic structures derived from resins and asphaltenes and suppress their further evolution toward condensed aromatic structures. This difference mainly originates from the different formation mechanisms of the active phases of the two catalysts. For aromatic heavy components, the conversion process usually follows a continuous reaction path of "hydrogenation activation—bridge-bond cleavage—radical stabilization—further cracking." First, the condensed-ring aromatic structures in resins and asphaltenes undergo partial hydrogenation under the action of active hydrogen, reducing the electron cloud density of the aromatic system and weakening the bond energies of inter-ring bridges and side-chain bonds; subsequently, these weakened bonds break, generating smaller aromatic radical fragments; finally, these radicals are rapidly stabilized by active hydrogen, avoiding secondary condensation and polymerization reactions. Because OMS can continuously provide a higher concentration of hydrogen radicals, it is more favorable for the above process. On the one hand, it promotes the hydrogenation saturation of condensed-ring aromatic structures, making the aromatic cores more susceptible to cracking; on the other hand, it rapidly hydrogenates radical intermediates, significantly inhibiting condensation reactions and the formation of coke precursors, thereby increasing the yield of light aromatic hydrocarbons and reducing heavy residues. From the chromatographic results, the intensities of low-retention-time aromatic peaks in the OMS products were generally higher than those in OMO, while the decrease in the heavy background in the high-retention-time region was also greater, indicating that OMS not only promoted the depolymerization of resins and asphaltenes but also increased the degree of deep conversion of aromatic structures. Especially in the M16VR system, which had the highest degree of heaviness, the advantage of OMS was most obvious, proving that it has stronger hydrocracking ability for highly condensed aromatic

structures and asphaltene aggregates. Therefore, it can be considered that OMS, through faster formation of a highly dispersed MoS2 active phase, more efficient hydrogen activation ability, and stronger radical stabilization, achieved deeper resin/asphaltene conversion and lightening of aromatic heavy components than OMO, thereby exhibiting superior slurry-phase hydrocracking catalytic performance.

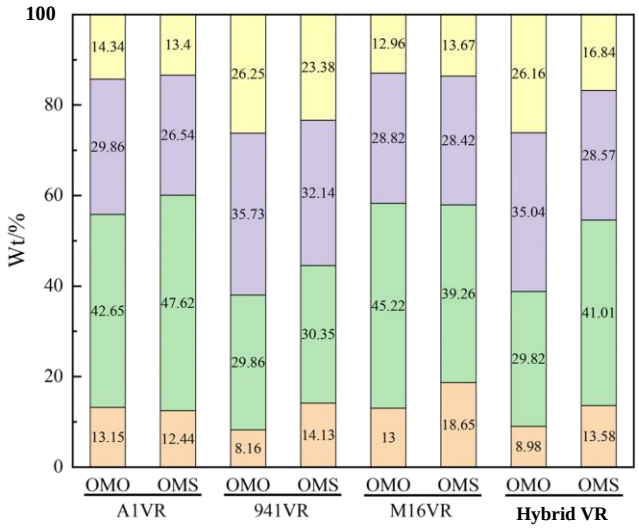

Figure 5. *Boiling-range distribution of hydrogenation products from four typical residues with different catalysts.*

Figure 5 shows the high-temperature simulated distillation results of the hydrogenation products obtained from four typical residue feedstocks after slurry-phase hydrocracking. According to the simulated distillation results, the liquid products were divided into four fractions: gasoline, diesel, wax oil, and residue [17]. Overall, all four residue feedstocks achieved lightening conversion to varying degrees after hydrocracking, and diesel and wax oil still occupied the main proportions of the liquid products, but different catalysts showed obvious effects on the distribution of each fraction. Especially under the action of the OMS catalyst, the proportions of light fractions such as gasoline and diesel in the liquid products increased overall, while the contents of heavy fractions such as wax oil and residue generally decreased, further indicating that OMS has stronger hydrocracking activity and higher conversion ability for heavy components. The A1VR feedstock obtained relatively high diesel yields after hydrogenation with both catalysts. With OMO catalysis, the mass fractions of gasoline, diesel, wax oil, and residue in the first liquid product were 13.15 wt%, 42.65 wt%, 29.86 wt%, and 14.34 wt%, respectively; with OMS, the diesel yield further increased to 47.62 wt%, an increase of nearly 5 percentage points compared with OMO, while wax oil and residue decreased to 26.54 wt% and 13.40 wt%, respectively. Although the gasoline yield decreased slightly, the total light fraction (gasoline + diesel) increased from 55.80 wt% to 60.06 wt%, indicating that OMS promoted the conversion of medium- and high-boiling-point components into the diesel fraction. From the perspective of the refining industry, diesel is usually one of the most important middle-distillate products in refineries; higher diesel selectivity means that A1VR can obtain higher economic value under OMS catalysis. For the 941VR feedstock, the slurry-phase hydrocracking upgrading effect of OMS was even more obvious. Under OMO catalysis, the gasoline and diesel yields were 8.16 wt% and 29.86 wt%, respectively, whereas under OMS catalysis they increased to 14.13 wt% and 30.35 wt%. At the same time, the wax oil and residue yields decreased from 35.73 wt% and 26.25 wt% to 32.14 wt% and 23.38 wt%, respectively. Among them, the gasoline yield increased by 73%, indicating that OMS can effectively promote deep cracking of large-molecular aromatic structures and asphaltene components in 941VR. In the aforementioned full-product simulated distillation analysis, 941VR showed a relatively high residue tendency, while within the liquid products, OMS could still be observed to significantly increase the proportion of light fractions, indicating that this catalyst can not only suppress the formation of coke precursors but also further promote the conversion of liquid heavy components into low-boiling-point fractions. Therefore, for heavy residue feedstocks with complex composition and high aromaticity, OMS exhibits stronger deep conversion ability. The M16VR feedstock showed a distribution characteristic slightly different from the previous two feedstocks. Under OMO catalysis, the diesel yield reached 45.22 wt%, whereas under OMS catalysis the diesel yield decreased slightly to 39.26 wt%, but the gasoline yield increased significantly from 13.00 wt% to 18.65 wt%, an increase of 43.5%. At the same time, the wax oil yield remained basically stable, and the residue yield changed little. This indicates that OMS further promoted the cracking conversion of the diesel fraction into the lighter gasoline fraction, that is, the cracking depth further increased. Although the diesel proportion decreased somewhat, the total light fraction yield changed from 58.22 wt% to 57.91 wt%, basically remaining at a comparable level, while the product structure clearly shifted toward high-value gasoline. Considering that gasoline products usually have higher market value, this product distribution is also positive for improving the economic benefits of heavy-oil upgrading. The HybridVR feedstock fully reflected the comprehensive advantages of the OMS catalyst. With OMO, the yields of gasoline, diesel, wax oil, and residue were 8.98 wt%, 29.82 wt%, 35.04 wt%, and 26.16 wt%, respectively; with OMS, the distribution of each fraction changed markedly: gasoline increased to 13.58 wt%, diesel increased to 41.01 wt%, while wax oil and residue decreased to 28.57 wt% and 16.84 wt%, respectively. Among them, the diesel yield increased by 11.19 percentage points, and the residue yield decreased by 9.32 percentage points, showing an extremely significant lightening effect. The total light fraction yield increased substantially from 38.80 wt% to 54.59 wt%, an increase of more than 15 percentage points.

This indicates that OMS can effectively promote the synergistic conversion of heavy components with different structures in mixed residue systems and improve the overall utilization efficiency of the feedstock. For industrial refineries, HybridVR is usually closer to actual processing feedstocks; therefore, this result indicates that the application potential of OMS in actual industrial feedstocks is particularly prominent.

From the overall trends, the OMS catalyst exhibited better hydrocracking performance than OMO in all four residue systems. Compared with OMO, OMS generally increased the proportions of light fractions such as gasoline and diesel while reducing the contents of high-boiling-point components such as wax oil and residue, indicating that it can achieve deeper molecular cracking and a higher degree of feedstock conversion. This is mainly attributed to the fact that OMS can directly form a highly dispersed MoS_2 nanoactive phase during the reaction, with faster activation, more edge active sites, and stronger activation ability for hydrogen molecules. Large amounts of active hydrogen can promptly stabilize the radical intermediates generated during cracking, promoting bridge-bond cleavage, side-chain removal, and depolymerization of inter-aromatic-ring linking structures, thereby improving the conversion efficiency of heavy components into light oils. In addition, the nano-MoS_2 sheets formed by OMS have higher dispersibility and better contact efficiency with the feedstock, which can significantly enhance the catalytic effect on difficult-to-convert components such as asphaltenes and resins, thus exhibiting superior hydrocracking activity.

4. Conclusions

All four feedstocks contained large amounts of heavy saturated hydrocarbons and condensed-ring aromatics. After hydrogenation, both saturated and aromatic hydrocarbon chromatograms showed enhanced low-retention-time peaks and weakened high-retention-time UCM backgrounds, indicating effective chain scission and depolymerization of heavy components and their migration toward lower carbon numbers. OMS was overall superior to OMO: it gave higher light-peak groups and n-alkane peaks and greater attenuation of the heavy background; in 941VR, the broad peak in the 20–50 min region was almost eliminated, indicating that OMS has stronger conversion ability for high-molecular-weight saturated hydrocarbons and condensed-ring aromatics. The fraction distribution was consistent with the chromatographic patterns. OMS generally increased gasoline and diesel yields and reduced wax oil and residue contents; the total light fraction of HybridVR increased from 38.80 wt% to 54.59 wt%, and the residue decreased to 16.84 wt%. The advantage of OMS originates from its self-sulfiding precursor, which can rapidly form a highly dispersed MoS2 active phase with abundant edge sites. The sufficient supply of active hydrogen can promptly stabilize radicals and inhibit condensation, thereby achieving deeper hydrocracking and heavy-oil lightening.

Abbreviations

OMO	Oil-soluble Molybdenum Oxidized Catalyst
OMS	Oil-soluble MoS_2 Catalyst

Author Contributions

Yidi Wang: Writing – original draft, Writing – review & editing

Funding

This work is supported by the Key R&D Program of Shandong Province, China (Nos. 2025ZLGX08 and 2024CXGC010408).

Data Availability Statement

The data supporting the outcome of this research work has been reported in this manuscript.

Conflicts of Interest

The authors declare no conflicts of interest.

References

[1] B. Liu, H. Lv, X. Cui, G. Sun, X. Zhang, B. Dong, Y. Li, Y. Pan, Y. Chai, C. Liu. Preparation of presulfided oil-soluble NiMo catalyst for slurry bed hydrocracking of vacuum residue. Chem Eng J 2024; 498: 155166. https://doi.org/10.1016/j.cej.2024.155166

[2] D. Guan, G. Cai, L. Zhang. Dual-objective optimization for petroleum molecular reconstruction based on property and composition similarities. AIChE J 2023; 69: e18108. https://doi.org/10.1002/aic.18108

[3] Y.-D. Wang, X. Zhang, X.-Y. Feng, B. Liu, Y. Pan, G.-Z. Sun, H.-Y. Lv, F.-Y. Tian, B. Dong, Y.-C. Li, C.-G. Liu, Y.-M. Chai. Comparing the thermal processing with slurry phase hydroupgrading to increase the yields of distillates of Arabian heavy crude oil. Petrol Sci 2026; 23: 966-978. https://doi.org/10.1016/j.petsci.2025.11.032

[4] T. A. Al-Attas, S. A. Ali, M. H. Zahir, Q. Xiong, S. A. Al-Bogami, Z. O. Malaibari, S. A. Razzak, M. M. Hossain. Recent Advances in Heavy Oil Upgrading Using Dispersed Catalysts. Energy Fuels 2019; 33: 7917-7949. https://doi.org/10.1021/acs.energyfuels.9b01532

[5] G. Bellussi, G. Rispoli, A. Landoni, R. Millini, D. Molinari, E. Montanari, D. Moscotti, P. Pollesel. Hydroconversion of heavy residues in slurry reactors: Developments and perspectives. J Catal 2013; 308: 189-200. https://doi.org/10.1016/j.jcat.2013.07.002

[6] J.-M. Lu, Y.-F. Wang, Z.-Y. Zhou, J.-X. Wu, Y.-H. Zhang, L.-Z. Zhang, Q. Shi, S.-B. He, C.-M. Xu. Molecular transformation of heavy oil during slurry phase hydrocracking process: Influences of operational conditions. Petrol Sci 2025; 22: 884-893. https://doi.org/10.1016/j.petsci.2024.09.002

[7] R. Prajapati, K. Kohli, S. K. Maity. Slurry phase hydrocracking of heavy oil and residue to produce lighter fuels: An experimental review. Fuel 2021; 288: 119686. https://doi.org/10.1016/j.fuel.2020.119686

[8] Y. Wang, J. Lu, X. Zhang, X. Zhang, B. Zhang, J. Wu, D. Guan, Y. Zhang, J. Chen, X. Feng, Y. Zhang, Z. Zhou, L. Zhang, Q. Shi. Molecular transformation of heavy oil during slurry phase hydrocracking process: A comparison between thermal cracking and hydrocracking. Fuel 2023; 351: 128981. https://doi.org/10.1016/j.fuel.2023.128981

[9] D. D. Pham, T. M. Nguyen, T. H. Ho, Q. V. Le, D. L. T. Nguyen. Advancing hydrodesulfurization in heavy Oil: Recent developments, challenges, and future prospects. Fuel 2024; 372: 132082. https://doi.org/10.1016/j.fuel.2024.132082

[10] S. S. Bello, C. Wang, M. Zhang, H. Gao, Z. Han, L. Shi, F. Su, G. Xu. A Review on the Reaction Mechanism of Hydrodesulfurization and Hydrodenitrogenation in Heavy Oil Upgrading. Energy Fuels 2021; 35: 10998-11016. https://doi.org/10.1021/acs.energyfuels.1c01015

[11] H.-B. Moon, J.-H. Lee, H.-T. Kim, J.-W. Lee, B.-H. Lee, C.-H. Jeon. Effect of high-pressure pyrolysis on syngas and char structure of petroleum coke. Energy 2024; 299: 131348. https://doi.org/10.1016/j.energy.2024.131348

[12] Q. Shi, Y. Zhang, K. H. Chung, S. Zhao, C. Xu. Molecular Characterization of Fossil and Alternative Fuels Using Electrospray Ionization Fourier Transform Ion Cyclotron Resonance Mass Spectrometry: Recent Advances and Perspectives. Energy Fuels 2021; 35: 18019-18055. https://doi.org/10.1021/acs.energyfuels.1c01671

[13] Q. Shi, S. Zhao, Z. Xu, K. H. Chung, Y. Zhang, C. Xu. Distribution of Acids and Neutral Nitrogen Compounds in a Chinese Crude Oil and Its Fractions: Characterized by Negative-Ion Electrospray Ionization Fourier Transform Ion Cyclotron Resonance Mass Spectrometry. Energy Fuels 2010; 24: 4005-4011. https://doi.org/10.1021/ef1004557

[14] B. Liu, K. Zhao, Y. Chai, Y. Li, D. Liu, Y. Liu, C. Liu. Slurry phase hydrocracking of vacuum residue in the presence of presulfided oil-soluble MoS2 catalyst. Fuel 2019; 246: 133-140. https://doi.org/10.1016/j.fuel.2019.02.114

[15] D. Liu, H. Du, J. Zhang, G. Que. Reverse Microemulsion Synthesis and Characterization of Nano Nickel Sulfide Catalyst for Residue Slurry-Phase Hydrocracking. Energy Fuels 2015; 29: 3353-3358. https://doi.org/10.1021/acs.energyfuels.5b00067

[16] Y. Wang, J. Wu, L. Xie, M. Yuan, Z. Jing, S. Pan, W. Zhang, Y. Zhang, Q. Shi. Identification and Geochemical Implication of Sulfur Compounds in an Immature Lacustrine Shale Oil. Energy Fuels 2023; 37: 12946-12952. https://doi.org/10.1021/acs.energyfuels.3c01860

[17] H. Du, D. Liu, M. Li, P. Wu, Y. Yang. Effects of the Temperature and Initial Hydrogen Pressure on the Isomerization Reaction in Heavy Oil Slurry-Phase Hydrocracking. Energy Fuels 2015; 29: 626-633. https://doi.org/10.1021/ef5024143